

# DyQ-VLA: Temporal-Dynamic-Aware Quantization for Embodied Vision-Language-Action Models

\*Zihao Zheng<sup>1</sup>, \*Hangyu Cao<sup>2</sup>, Sicheng Tian<sup>3</sup>, Jiayu Chen<sup>1</sup>, Maoliang Li<sup>1</sup>, Xinhao Sun<sup>4</sup>, Hailong Zou<sup>1</sup>, Zhaobo Zhang<sup>1</sup>, Xuanzhe Liu<sup>1</sup>, Donggang Cao<sup>1</sup>, Hong Mei<sup>1</sup>, †Xiang Chen<sup>1</sup>

**Abstract**— Vision-Language-Action (VLA) models are dominant in embodied intelligence but are constrained by inference overheads. While model quantization alleviates these bottlenecks for edge deployment, static quantization approaches remain suboptimal for VLAs due to two critical challenges: (1) Temporal-dynamic sensitivity, where fixed precision wastes resources by ignoring stage-varying error tolerances; and (2) Real-time allocation, where identifying real-time sensitivity to guide bit allocation remains unsolved. To address these challenges, we propose *DyQ-VLA*, a dynamic quantization framework for VLAs. Specifically, a sensitivity-aware switching strategy leverages real-time kinematic proxies to trigger the bit-width switch, while a kinematic-guided module dynamically allocates the optimal bit-width. Experiments show that *DyQ-VLA* requires only 30.9% of the original memory footprint while maintaining 99.5% of its original performance, achieving 1.49× simulation and up to 1.43× real-world speedups.

## I. INTRODUCTION

Vision-Language-Action (VLA) models have emerged as the dominant paradigm in embodied intelligence [1], [2], achieving exceptional versatility by translating visual perceptions and textual instructions into precise robotic actions [3]–[5]. Such versatility inherently entails substantial computation and memory overheads, which constrain their real-time deployment on resource-constrained edge devices [1], [2].

To alleviate these overheads, recent research has adapted Large Language Models (LLMs) optimization techniques for VLA architecture, including: compression-based optimizations, exemplified by token pruning [6]–[8] to mitigate token-level redundancy; runtime optimizations, including speculative decoding [9] for parallel generation, caching [10], [11] to reuse cached states, and layer skipping [12]–[14] to bypass computations; architectural innovations [15]–[17] that redesign model structures to realize real-time inference.

Complementing these methods, model quantization as a well-established and effective approach reduces memory footprints and accelerates inference by employing efficient low-bit integer computation. Notably, some representative techniques such as GPTQ [18], AWQ [19], APTQ [20], and SmoothQuant [21] achieve significant compression while maintaining near-lossless accuracy across diverse tasks.

\* Equal Contribution.

<sup>1</sup> School of Computer Science, Peking University, Beijing, China.

<sup>2</sup> School of Software Engineering, South China University of Technology, Guangzhou, China.

<sup>3</sup> School of Artificial Intelligence, Beijing Normal University, Beijing, China.

<sup>4</sup> School of Electronics Engineering and Computer Science, Peking University, Beijing, China.

† Corresponding Author: Xiang Chen.<xiaang.chen@pku.edu.cn>

Inspired by the success of quantization in LLMs, recent research has adapted these techniques to VLAs. QVLA [22] evaluates the impact of per-channel quantization on final action accuracy, allocating bit-widths at the channel level accordingly. Moreover, to push these compression limits, SQAP-VLA [23] synergistically co-optimizes quantization and pruning to accelerate VLA inference.

However, unlike LLMs, VLAs act as embodied agents in the physical world, presenting two critical quantization challenges: (1) **Temporal-dynamic quantization sensitivity**: VLA sensitivity fluctuates drastically over time; a negligible quantization error (e.g., a 1mm deviation) is harmless during coarse-grained movements, but often becomes fatal in precision manipulation. Governed by peak sensitivity, static quantization must maintain high precision throughout, wasting substantial computational resources to prevent task failure. (2) **Real-time bit allocation**: While VLA quantization sensitivity fluctuates across execution steps, exploiting these temporal dynamics remains an open challenge. Specifically, existing methods lack a reliable lightweight proxy for instantaneous sensitivity, which prevents optimal dynamic bit allocation without prohibitive runtime overhead.

To address these challenges, we first profile the quantization sensitivity of VLA models, revealing their temporal-dynamic nature. We find that identical quantization noise affects task outcomes differently depending on the execution stage, with coarse-grained movements showing much higher error tolerance. Furthermore, we demonstrate a strong correlation between this temporal-dynamic sensitivity and kinematic metrics. Consequently, by monitoring the real-time kinematic states of the robotic arm during inference, we can accurately estimate the instantaneous sensitivity magnitude.

Motivated by these insights, we propose *DyQ-VLA*, a dynamic quantization framework for VLA. *DyQ-VLA* integrates two synergistic components: (1) a sensitivity-aware switching strategy that monitors real-time kinematic proxies to dictate the precise timing for bit-width transitions; and (2) a kinematic-guided bit allocation module that infers instantaneous sensitivity from kinematic metrics to dynamically determine the optimal bit-width. Both simulated and real-world evaluations confirm that *DyQ-VLA* achieves superior performance and efficiency. Notably, its orthogonal, plug-and-play design augments static methods, facilitating VLA edge deployment. Overall, our contributions are threefold:

- We reveal the temporal-dynamic nature of VLA quantization sensitivity and empirically establish kinematic metrics as reliable, real-time proxies for sensitivity identification.

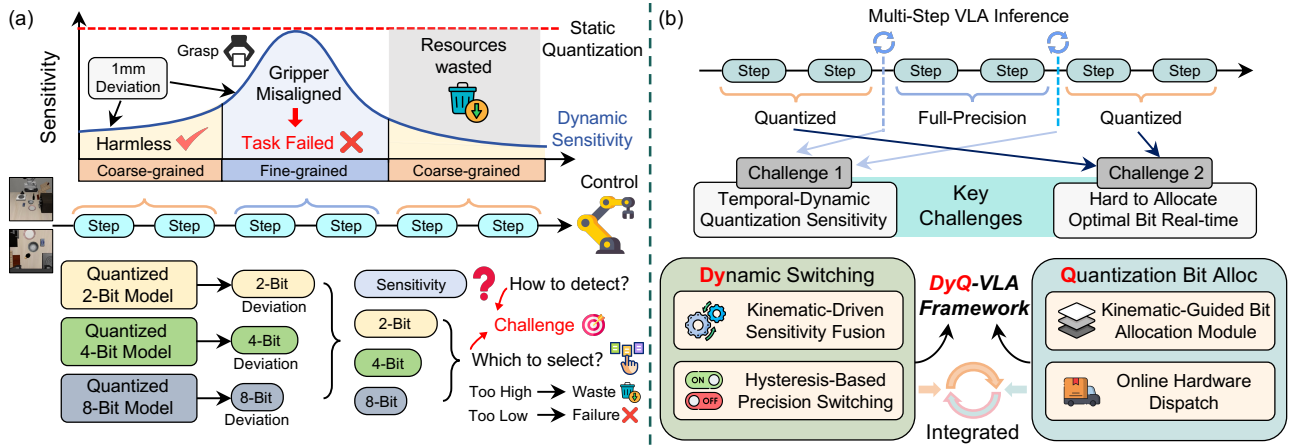


Fig. 1. (a) Challenges for VLA Model Quantization. (b) Overview of the proposed *DyQ-VLA* Framework

- We propose *DyQ-VLA*, a dynamic quantization framework for VLA, integrating a sensitivity-aware precision switching strategy and a kinematic-guided bit allocation module.
- We validate *DyQ-VLA*'s efficient, near-lossless performance in simulated and real-world experiments, establishing a novel paradigm for real-time edge deployment.

Specifically, *DyQ-VLA* retains 99.5% of baseline performance using merely 30.9% memory, accelerating simulation and real-world tasks by  $1.49\times$  and up to  $1.43\times$ , respectively.

## II. PRELIMINARY

### A. VLA Models

1) **Model Architecture:** VLA models [3]–[5] implement an embodied policy  $\pi_\theta$  through three components: a vision encoder for visual embeddings, an LLM Backbone for multimodal fusion and reasoning, and an action detokenizer that reconstructs predicted tokens into control commands.

2) **Autoregressive Inference:** A VLA policy  $\pi_\theta$  models action execution as a generative sequence of  $L$  discrete tokens  $A_t = \{a_1, \dots, a_L\}$ . Specifically, the  $k$ -th token  $a_k$  is conditioned on the visual observation  $I_t$ , language instruction  $P$ , current state  $x_t$ , and previously generated tokens  $a_{1:k-1}$ . This autoregressive process is formulated as Eq. (1).

$$\pi_\theta(A_t | I_t, x_t, P) = \prod_{k=1}^L P_\theta(a_k | a_{1:k-1}, I_t, x_t, P) \quad (1)$$

### B. Model Quantization

1) **Quantization for VLA Models:** To optimize efficiency, uniform quantization [18], [19], [21] maps a high-precision tensor  $X$  to a  $b$ -bit integer  $Q(X)$ , formulated as Eq. (2).

$$Q(X) = \text{clamp} \left( \left\lfloor \frac{X}{s} \right\rfloor + z, 0, 2^b - 1 \right) \quad (2)$$

where  $s$  and  $z$  denote the scale and zero-point. This process yields a reconstructed approximation  $\hat{X} = s \cdot (Q(X) - z)$  and introduces a local error  $e = X - \hat{X}$ .

2) **Challenge for VLA Model Quantization:** In closed-loop VLA control,  $e$  drives the recursive state deviation  $\Delta x_t$  like (3), where  $\mathbf{J}_\pi$  and  $\mathbf{J}_\tau$  denote highly dynamic policy sensitivity and environmental gain across execution steps. To prevent dynamic amplification of the error  $\mathbf{J}_\tau(\mathbf{J}_\pi \cdot e)$  during critical manipulation phases, static quantization must globally minimize  $e$ . This mismatch between static precision and dynamic noise tolerance introduces severe computational redundancy during coarse motions. Meanwhile, the recursive term  $\mathbf{J}_\tau \Delta x_{t-1}$  continually compounds these local errors into fatal trajectory drift. Thus, static paradigms fundamentally fail to balance efficiency and long-horizon stability.

$$\Delta x_t \approx \mathbf{J}_\tau \Delta x_{t-1} + \mathbf{J}_\tau(\mathbf{J}_\pi \cdot e) \quad (3)$$

## III. OBSERVATION AND MOTIVATION

This section explores the temporal-dynamic sensitivity of quantization and its correlation with kinematic metrics. Establishing this correlation provides the fundamental basis for our dynamic quantization framework design.

### A. Temporal Dynamics of VLA's Quantization Sensitivity

**Motivation ①:** Conventional static quantization methods are bottlenecked by the peak sensitivity of the model across an entire task. This worst-case assumption forces uniform high precision, wasting substantial computational resources.

To address this limitation, we highlight that the quantization sensitivity of VLA models is inherently dynamic. During robotic manipulation, the precision needs vary significantly across different execution steps. For instance, fine-grained manipulation demands strict accuracy for precise object handling (e.g., grasping or insertion), whereas coarse-grained free-space movements maintain significant error resilience.

To systematically investigate this dynamic characteristic and quantify the temporal-dynamic sensitivity, we conduct a step-wise perturbation analysis. This analysis evaluates how uniform quantization noise impacts task success across different execution steps. Specifically, to evaluate the OpenVLA model [3] on the LIBERO benchmark [24], we first collect a comprehensive set of successful full-precision (BF16) execution trajectories to serve as our baseline. Using these

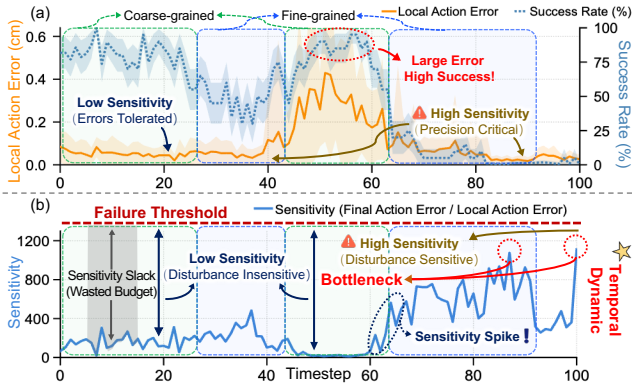


Fig. 2. (a) Non-linear relationship between local action error and success rate. (b) Temporal-dynamic profiling of the sensitivity metric

trajectories, we conduct a step-wise perturbation analysis by injecting a single 4-bit (W4A4) quantized action at each time step  $t$ . Following this injection, the full-precision baseline policy resumes control for the remainder of the episode. To obtain a reliable task success rate, we repeat this perturbation across multiple episodes for every time step. We then plot the aggregated task success rate against the local action error, defined as  $e_t = \|p_{\text{int}4} - p_{\text{bf}16}\|_2$ . As shown in Fig. 2, the system retains strong error resilience during coarse movements. Counter-intuitively, even when the local quantization error  $e_t$  reaches its peak, the overall success rate remains consistently high. This clear decoupling of local action error from final task success confirms the inherently temporal-dynamic nature of quantization sensitivity.

To quantitatively capture this dynamic behavior, we define the sensitivity metric as  $s_t = D_T/e_t$ , where  $D_T$  is the terminal spatial deviation caused by the local perturbation at step  $t$ . We use this ratio because it quantifies how a local error at step  $t$  affects the final outcome, directly reflecting the model’s sensitivity at that specific moment. Consequently, these errors ultimately manifest as macroscopic deviations at trajectory completion, providing a reliable quantitative characterization of VLA model sensitivity to quantization noise. Fig. 2 (b) plots the temporal variation of  $s_t$ , revealing its highly dynamic characteristics throughout the task execution. Coarse movements are naturally robust to local noise, keeping  $s_t$  consistently low. In contrast, fine-grained manipulations are highly sensitive to these errors, triggering sudden  $s_t$  spikes that ultimately disrupt the entire task.

While  $s_t$  provides a rigorous ground-truth measurement, calculating it strictly requires terminal deviations available only after trajectory completion. This fundamental reliance on post-hoc analysis makes  $s_t$  unsuitable for real-time precision switching, creating a need for an instantaneous proxy. *Insights ①*: Our step-wise analysis uncovers a fundamental property: the quantization sensitivity of VLA models is inherently temporal-dynamic. As effectively captured by  $s_t$ , this sensitivity remains minimal during coarse movements but inevitably spikes during fine manipulation.

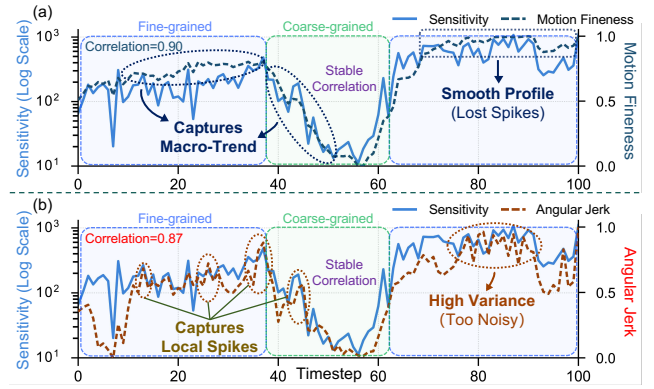


Fig. 3. (a) Smooth macro-alignment of Motion Fineness with sensitivity.(b) High Variance spike-alignment of Angular Jerk with sensitivity.

## B. Correlation Between Kinematic Metrics and Sensitivity

*Motivation ②*: While the temporal-dynamic nature of quantization sensitivity is evident, the strictly post-hoc calculation of  $s_t$  prohibits its direct application in real-time dynamic bit allocation. Bridging this gap requires an instantaneous proxy capable of tracking these sensitivity fluctuations.

Given that VLA models operate as embodied agents, we posit that kinematic metrics can act as a reliable proxy due to their tight coupling with the physical execution phase [25]. To verify this hypothesis, we investigate whether real-time kinematic metrics can effectively capture the fluctuations in instantaneous sensitivity. To capture both translational movements and rotational adjustments, we extract two complementary kinematic metrics: Motion Fineness ( $\mathcal{M}_t$ ) and Angular Jerk ( $\mathcal{J}_t$ ). Motion Fineness inversely scales the translational magnitude at step  $t$ , defined as  $\mathcal{M}_t = 1 - \|\mathbf{a}_t^{\text{xyz}}\|_2 / \mu_{\text{max}}$ , where  $\mu_{\text{max}}$  denotes the 95<sup>th</sup> percentile of historical magnitudes. Meanwhile, Angular Jerk directly measures the normalized rotational fluctuations between consecutive steps, defined as  $\mathcal{J}_t = \|\mathbf{a}_t^{\text{rot}} - \mathbf{a}_{t-1}^{\text{rot}}\|_2 / \nu_{\text{max}}$ , where  $\nu_{\text{max}}$  denotes the 95<sup>th</sup> percentile of historical angular jerks.

We then plot the normalized temporal trajectories of these proxies against the log-scaled sensitivity metric  $s_t$  (Fig. 3). The visual trajectories of both kinematic metrics closely track the sensitivity curve, demonstrating clear alignment in overall trends. Quantitatively, both kinematic metrics exhibit a strong temporal correlation with the ground-truth sensitivity, achieving correlation coefficients of  $r = 0.90$  for  $\mathcal{M}_t$  and  $r = 0.87$  for  $\mathcal{J}_t$ . Intuitively, fine-grained manipulation steps demand high execution accuracy, amplifying the system’s sensitivity. These strong correlations highlight the feasibility of using kinematic metrics as a real-time sensitivity indicator.

Although both metrics exhibit satisfactory concordance with sensitivity, they each demonstrate distinct but complementary properties. As shown in Fig. 3 (a), Motion Fineness ( $\mathcal{M}_t$ ) excels at tracking the macro-trend of temporal-dynamic sensitivity. By capturing continuous spatial movements,  $\mathcal{M}_t$  yields a smooth profile of the physical execution. However, this macroscopic smoothing inherently obscures transient fluctuations, thereby missing short-term spikes in sensitivity.

In contrast, Fig. 3 (b) demonstrates that Angular Jerk ( $\mathcal{J}_t$ )

reacts acutely to microscopic temporal variations. It successfully captures the sudden sensitivity spikes that occur during fine-grained manipulation. However, the high responsiveness of this metric naturally introduces significant variance, rendering the trajectory excessively jittery and noisy.

Results confirm that kinematic metrics act as effective proxies for temporal-dynamic sensitivity, laying the groundwork for dynamic precision switching. However, using either metric independently presents inherent limitations. Therefore, establishing a real-time proxy requires fusing these complementary kinematic signals, which inspires our design. *Insights ②*: Kinematic metrics exhibit a strong correlation with the temporal-dynamic quantization sensitivity of VLA models. These metrics manifest inherently complementary properties. Specifically,  $\mathcal{M}_t$  reliably captures stable macroscopic trends, while  $\mathcal{J}_t$  identifies microscopic variations.

#### IV. DyQ-VLA FRAMEWORK

This section details the proposed step-wise dynamic quantization framework, *DyQ-VLA*, which contains two components: (1) a sensitivity-aware precision switching strategy and (2) a kinematic-guided bit allocation module.

##### A. Sensitivity-Aware Precision Switching Strategy

###### 1) Static W-Quant and Dynamic A-Quant Paradigm:

To deploy VLA models on resource-limited edge devices, we adopt a static-weight, dynamic-activation (W4AX) quantization paradigm. Since dynamically swapping weights incurs severe bandwidth bottlenecks during the autoregressive decoding phase, we freeze the weights at 4-bit (INT4). This design choice facilitates the deployment of 7B-class VLA models on commodity memory while preserving the downstream task performance. Conversely, the step-wise activation dynamically alternates between a full-precision fallback (BF16) and a quantized state ( $X \in \{2, 4, 8\}$ ). Highly sensitive manipulation kinematics trigger a BF16 bypass to guarantee accuracy during critical physical interactions, whereas stable execution phases are dynamically quantized to lower bit-widths. This approach accelerates the execution of arithmetic logic units while avoiding weight swapping overhead, thus minimizing memory access latency.

2) *Kinematic-Driven Sensitivity Fusion*: To comprehensively guide the dynamic activation, we extract Motion Fineness ( $\mathcal{M}_t$ ) and Angular Jerk ( $\mathcal{J}_t$ ) as two complementary kinematic metrics, processing them through asymmetric temporal windows to respectively capture macroscopic trends and microscopic spikes (Fig. 4). Specifically, a broad macro-window  $W_{\text{macro}}$  averages the instantaneous Motion Fineness  $\mathcal{M}_i$  to track the stable macroscopic trend:  $\tilde{\mathcal{M}}_t = \frac{1}{W_{\text{macro}}} \sum_{i=t-W_{\text{macro}}+1}^t \mathcal{M}_i$ . In physical terms, lower values of this metric physically correspond to coarse-grained transits. Conversely, a tight micro-window  $W_{\text{micro}} (< W_{\text{macro}})$  averages the Angular Jerk  $\mathcal{J}_i$  to capture transient microscopic spikes:  $\tilde{\mathcal{J}}_t = \frac{1}{W_{\text{micro}}} \sum_{i=t-W_{\text{micro}}+1}^t \mathcal{J}_i$ . In physical terms, sudden surges in this micro-metric correspond to abrupt rotational adjustments. Because both  $\mathcal{M}_t$  and  $\mathcal{J}_t$  are inherently normalized against their historical percentiles (as defined in

Sec. III), they natively possess cross-task scale consistency. Thus, the unified sensitivity state, which harmonizes stable macroscopic trends with transient microscopic spikes, can be cleanly formulated via a convex combination without additional dynamic scaling:  $\mathcal{S}_t = \max(0, \lambda \mathcal{M}_t + (1 - \lambda) \tilde{\mathcal{J}}_t)$ .

3) *Hysteresis-Based Precision Switching*: Directly toggling between the full-precision state and various quantized states causes frequent context switching and severely degrades the overall system throughput. To mitigate these computational overheads and prevent rapid oscillations between precision states at the boundaries of sensitivity thresholds, we apply an asymmetric hysteresis operator to the unified target precision  $\hat{b}_t \in \{2, 4, 8, 16\}$ . We define a critical accuracy threshold  $\theta_{\text{fp}}$ . If  $\mathcal{S}_t > \theta_{\text{fp}}$ , the system enforces a full-precision bypass by directly setting  $\hat{b}_t = 16$ . Otherwise ( $\mathcal{S}_t \leq \theta_{\text{fp}}$ ), the system invokes the bit allocation module (Sec. IV-B) to determine the optimal quantization bit-width, assigning  $\hat{b}_t$  from the discrete subset  $\{2, 4, 8\}$ . Formally, a delay window  $K$  governs the dispatched bit-width  $b_t^*$ :

$$b_t^* = \begin{cases} \hat{b}_t, & \text{if } \hat{b}_t \geq b_{t-1}^* \\ \hat{b}_t, & \text{if } \max_{i \in [t-K+1, t]} (\hat{b}_i) \leq \hat{b}_t \\ b_{t-1}^*, & \text{otherwise} \end{cases} \quad (4)$$

This asymmetric design prioritizes accuracy by forcing immediate precision upgrades (for example, reverting to the BF16 format) whenever the target bit-width exceeds the active precision  $b_{t-1}^*$ . This mechanism instantly recovers the representational capacity of the model when complex action begins. Conversely, the delay window  $K$  serves as a temporal low-pass filter that maintains the previous high precision  $b_{t-1}^*$  to absorb transient sensory noise until a stable downgrade is confirmed, ultimately preventing catastrophic task failures. To eliminate the runtime memory overhead associated with deploying this continuous window, we introduce a low-cost stateful approximation that provides a sufficient condition for the stable and optimal selection of the bit-width.

##### B. Kinematic-Guided Bit Allocation Module

1) *Accuracy-Preserving Error Bounding*: Whenever the switching strategy initiates the quantized phase ( $\mathcal{S}_t \leq \theta_{\text{fp}}$ ), for efficient execution, the edge hardware is restricted to a discrete activation bit-width space  $\mathcal{B} = \{2, 4, 8\}$ . These power-of-two formats strictly align with native hardware instructions, avoiding the software emulation overhead typically associated with arbitrary precisions. To map the sub-critical sensitivity  $\mathcal{S}_t$  to the optimal hardware precision (Fig. 4 (b)), the dynamic allocation module identifies the minimal bit-width  $\hat{b}_t \in \mathcal{B}$  that satisfies a task-specific terminal accuracy-constrained deviation  $D_{\text{acc}}$ . The maximum allowable single-step action error shrinks as the manipulation sensitivity increases:  $\epsilon_a(\mathcal{S}_t) = D_{\text{acc}}/(\mathcal{S}_t + \eta)$ . This scaling occurs because minor deviations during critical phases can easily compound into an irreversible execution failure. This rigorous constraint structurally bounds the accumulated quantization error within the predefined accuracy region:

$$\hat{b}_t = \arg \min_{b \in \mathcal{B}} b \quad \text{s.t.} \quad \mathbb{E} \left[ \left\| \hat{\mathbf{a}}_t^{(b)} - \mathbf{a}_t^* \right\|_2 \right] \leq \epsilon_a(\mathcal{S}_t) \quad (5)$$

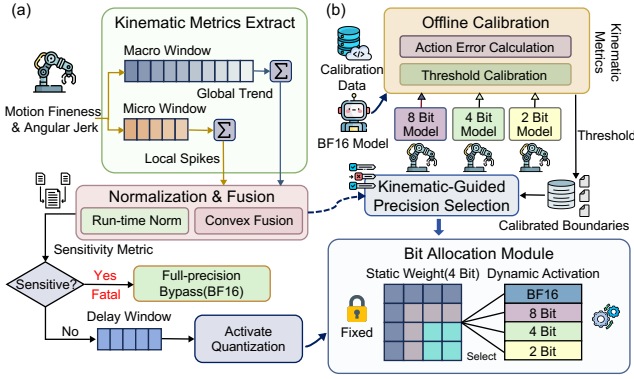


Fig. 4. Overview of the  $DyQ$ -VLA framework. (a) The sensitivity-aware precision switching strategy. (b) The kinematic-guided bit allocation module.

where  $\mathbf{a}_t^*$  and  $\hat{\mathbf{a}}_t^{(b)}$  denote the full-precision oracle (BF16) command and the quantized action command, respectively.

2) **Offline Threshold Calibration:** Predicting the exact action deviations caused by the quantization of VLA models is computationally intractable during inference due to compounding non-linearities across consecutive execution steps. To satisfy the accuracy bound without introducing online computational burdens, we derive a discrete mapping function  $\Phi: \mathcal{S}_t \mapsto \mathcal{B}$  via offline calibration. By executing the full-precision model on a representative calibration subset of successful trajectories, we quantify the actual local action deviation  $e_t^{(b)} = \|\hat{\mathbf{a}}_t^{(b)} - \mathbf{a}_t^*\|_2$ . We systematically identify critical intersections where the lower-bit quantization error consistently exceeds the accuracy bound  $\epsilon_a(\mathcal{S}_t)$ . These intersections define the precise interval boundaries within the quantized domain, denoted as  $\Theta = \{\theta_{2|4}, \theta_{4|8}\}$ .

3) **Online Hardware Dispatch:** At runtime, this error-bounding objective effectively reduces to a static piecewise mapping exclusively for the quantized subdomain  $[0, \theta_{fp}]$ , significantly minimizing computational complexity by operating as a constant-time lookup table:

$$\Phi(\mathcal{S}_t) = \begin{cases} 2, & \mathcal{S}_t \in [0, \theta_{2|4}] \\ 4, & \mathcal{S}_t \in (\theta_{2|4}, \theta_{4|8}] \\ 8, & \mathcal{S}_t \in (\theta_{4|8}, \theta_{fp}] \end{cases} \quad (6)$$

By mapping continuous kinematics directly to disjoint discrete regions, the function  $\Phi$  enables arbitrary, non-sequential precision jumps. This non-sequential flexibility is crucial for embodied tasks where the physical context can change drastically in a single step. For instance, transitioning from fine-grained manipulation to coarse-grained movement sharply reduces the corresponding sensitivity, enabling the system to drop from the BF16 state to 2-bit execution, thereby bypassing intermediate downgrades. For efficient deployment, a lightweight saturating counter (Alg. 1) approximates the sliding window. The previous high precision  $b_{t-1}^*$  is strictly preserved during upward jitter, as any target precision upgrade or new sensory spike ( $\hat{b}_t \geq b_{t-1}^* \vee \hat{b}_t > \bar{b}_{t-1}$ ) mandates a counter reset. Consequently, the dynamic bit-width allocation becomes a reliable low-cost operation, accelerating the inference runtime without introducing significant

### Algorithm 1 Stateful Hardware Dispatcher of $DyQ$ -VLA

**Input:** Kinematic means  $\tilde{\mathcal{M}}_t, \tilde{\mathcal{J}}_t$ ; params  $\Theta, \theta_{fp}, \lambda, K$ .

**State:** Counter  $c_{t-1} \in [0, K)$ ; active precision  $b_{t-1}^*$ ; max candidate  $\bar{b}_{t-1}$ .

- 1:  $\mathcal{S}_t \leftarrow \max(0, \lambda \tilde{\mathcal{M}}_t + (1 - \lambda) \tilde{\mathcal{J}}_t)$
- 2:  $\hat{b}_t \leftarrow 16 \cdot \mathbb{I}(\mathcal{S}_t > \theta_{fp}) + \Phi(\mathcal{S}_t; \Theta) \cdot \mathbb{I}(\mathcal{S}_t \leq \theta_{fp})$
- 3: **if**  $\hat{b}_t \geq b_{t-1}^*$  **then**
- 4:      $(b_t^*, c_t, \bar{b}_t) \leftarrow (\hat{b}_t, 0, \hat{b}_t)$
- 5: **else**
- 6:      $\bar{b}_t \leftarrow \max(\hat{b}_t, \bar{b}_{t-1} \cdot \mathbb{I}(c_{t-1} > 0))$
- 7:      $c_t \leftarrow c_{t-1} \cdot \mathbb{I}(\bar{b}_t = \bar{b}_{t-1}) + 1$
- 8:      $(b_t^*, c_t) \leftarrow (\bar{b}_t \cdot \mathbb{I}(c_t = K) + b_{t-1}^* \cdot \mathbb{I}(c_t < K), c_t \bmod K)$
- 9: **end if**
- 10: **return**  $b_t^*$

memory footprint or scheduling overhead.

### V. $DyQ$ -VLA FRAMEWORK IMPLEMENTATION

This section details the implementation of the  $DyQ$ -VLA framework, focusing on the hardware-native operator mapping and the asynchronous computation flow.

#### A. Hardware Mapping and Mixed-Precision Backend

Implementing dynamic multi-precision quantization ( $\mathcal{B} \in \{2, 4, 8\}$ ) requires specific system optimizations to mitigate memory bandwidth bottlenecks during the autoregressive action token generation of VLA models.

To achieve efficient quantitative computing, we first design and optimize quantization operators. A key feature of the quantization operators is the use of INT4-pinned weights across all precision settings. By maintaining the weights as densely packed INT4 tensors in the GPU's Global Memory (GMEM), the system could maximize the bandwidth utilization. To eliminate the global memory access overhead of dynamic activation quantization, operations including scaling, quantization to bit-width  $\mathcal{B}$ , and GMEM packing are fused into the MMA kernel. This integration effectively eliminates the need for additional load/offload passes.

During the forward passes of general matrix multiply (GEMM) operations, the packed activations for  $\mathcal{B} \in \{4, 8\}$  utilize native INT4 and INT8 Tensor Cores via specialized kernels. For  $\mathcal{B} = 8$ , the weights stored in the INT4 format are decompressed on the fly into the INT8 format within registers to match the W8A8 computational pipeline. This approach utilizes high-precision activation modeling while retaining the memory efficiency of 4-bit storage. For  $\mathcal{B} = 2$ , the backend packs activations in the GMEM to halve the read bottlenecks, subsequently unpacking them into the INT4 format for W4A4 computation using optimized bitwise operations. This tight coupling of memory-bound fetching with zero-overhead decompression ensures that precision reduction translates directly into end-to-end speed gains.

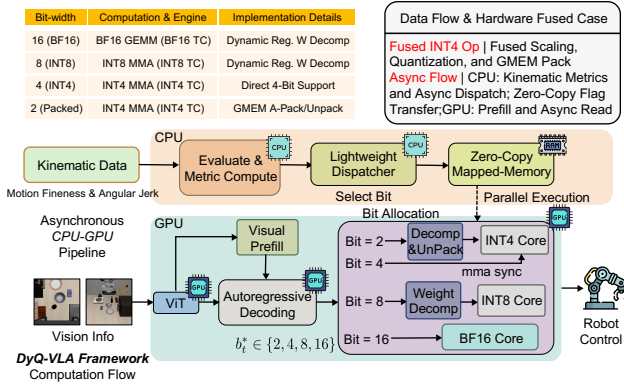


Fig. 5. System Implementation of *DyQ-VLA* Framework

## B. End-to-End Asynchronous Computation Flow

To prevent dynamic precision switching from introducing scheduling overhead, the lightweight dispatcher is structurally decoupled from the model via an asynchronous CPU-GPU pipeline. The target bit-width  $b_t^*$  is determined per step or action chunk instead of per token, avoiding severe kernel launch delays during the decoding process. At each control step  $t$ , the host and the device operate concurrently to maximize throughput. While the GPU handles the computationally intensive visual prefill phase, the CPU asynchronously processes the proprioceptive data to compute the kinematic metrics ( $\mathcal{M}_t, \mathcal{J}_t$ ). These metrics are subsequently fed into the dispatcher to evaluate the sensitivity  $\mathcal{S}_t$  and select the optimal bit-width  $b_t^* \in \{2, 4, 8, 16\}$ , where 16 denotes fallback.

Because the dispatcher relies on simple scalar arithmetic, the execution time remains negligible at the microsecond scale. To achieve zero-latency synchronization, the selected bit-width  $b_t^*$  is directly written to the Zero-Copy mapped memory, completely bypassing blocking host-to-device transfers. Upon transitioning to the autoregressive decoding phase, the GPU reads this flag to route the execution to the corresponding pre-compiled CUTLASS kernel. Overlapping the kinematic evaluation on the CPU with the visual prefill on the GPU effectively hides the entire scheduling overhead of the quantization process. Consequently, this architecture enables deep hardware acceleration while maintaining the strict control frequency essential for reliable robotic deployment.

## VI. EXPERIMENTS

### A. Setup

1) **Hardware and Environments:** We evaluate *DyQ-VLA* across diverse manipulation tasks within the LIBERO [24] simulation benchmark and physical real-world environments. All system-level evaluations are conducted on an NVIDIA A100 GPU paired with an Intel Xeon Silver 4410T CPU.

2) **Models:** We use OpenVLA [3] as the base model. Because its LLM backbone generates actions token-by-token without independent modules, this homogeneous architecture avoids downstream interference. This provides a clean setup to evaluate the proposed dynamic quantization framework.

3) **Baselines:** To isolate the efficacy of dynamic bit allocation, we compare *DyQ-VLA* against mainstream and domain-specific baselines. For standard static fixed-precision quantization, we compare against SmoothQuant [21]. We also evaluate against QVLA [22], a state-of-the-art quantization method tailored for VLAs. The unquantized BF16 model serves as the performance upper bound. We also perform an internal ablation by omitting the kinematic-guided module.

4) **Evaluation Metrics:** We evaluate both task performance and deployment efficiency. Task completion is measured by Success Rate (%), while inference efficiency is assessed using Peak Memory (GB) and End-to-End Latency (ms). Aligned with our GPU hardware mapping and asynchronous computation flow, latency strictly measures the complete execution time from initial input to final action output to reflect real-time responsiveness for robot control.

### B. Evaluation Results

1) **Simulation Results:** We evaluate *DyQ-VLA* across four LIBERO task suites (40 tasks, 200 trials each). As reported in Tab. I, *DyQ-VLA* achieves a  $1.47\times \sim 1.51\times$  speedup and reduces peak memory by 10.5 GB compared to the full-precision model. While naive SmoothQuant offers higher speedups at the cost of severe success rate (SR) degradation, *DyQ-VLA* maintains a competitive 76.1% average SR. Notably, it yields a 0.1% absolute SR improvement over the QVLA baseline despite a marginal memory overhead, preserving 99.5% of the full-precision performance.

The advantages of our dynamic framework are evident in its task-specific behaviors. To prevent trajectory drift during precision-critical Angular Jerk spikes, *DyQ-VLA* dynamically reverts to the BF16 state. In the LIBERO-Spatial suite, this targeted fallback achieves lossless precision routing, preserving an 84.7% success rate with a conservative  $1.51\times$  speedup. Conversely, the LIBERO-Long suite contains extensive macroscopic translations with low Motion Fineness. During these stable phases, the dispatcher assigns low-bit activation states (e.g.,  $X = 2$ ) to alleviate memory bandwidth bottlenecks. Consequently, *DyQ-VLA* achieves a substantial  $1.49\times$  speedup and a 53.4% success rate. This effectively demonstrates the capability of dynamic precision switching to balance latency and execution accuracy.

2) **Real-World Results:** To validate generalizability, we construct a tabletop manipulation setup using a 6-DoF robotic arm equipped with a 1-DoF parallel gripper and a primary-view RGB camera. We design physical tasks across three complexity levels: atomic grasping of simple objects, spatial displacement to move objects into designated containers, and composite sequential tasks requiring long-horizon multi-step planning. To bridge the sim-to-real gap, we collect 400 human demonstration episodes per task category using a physical teach pendant operating at a 10 Hz control frequency. We fine-tune the model using Quantized Low-Rank Adaptation to preserve the static-weight paradigm. Specifically, we inject low-rank adapters with a rank of 32 and a dropout rate of 0.05 into the attention projections of the backbone, keeping the pre-trained 4-bit base weights

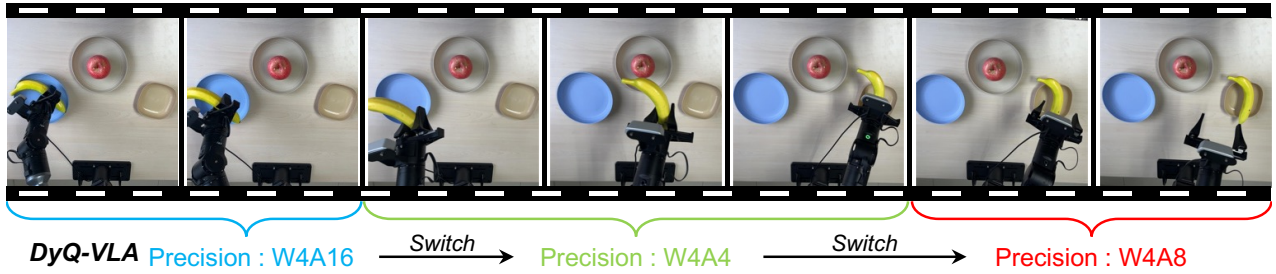


Fig. 6. A Case of *DyQ-VLA* Framework Completing Real-World Tasks (Task Name: Pick up the Banana and Put It into the Khaki Bowl)

frozen. During inference, a client-server architecture enables the server to autoregressively decode actions while the client executes the joint commands. Across the three task categories (with unquantized baseline success rates of 86.7%, 76.7%, and 70.0%), our method achieves a  $1.32\times \sim 1.43\times$  end-to-end latency speedup. As shown in Tab. II, *DyQ-VLA* remains robust in the physical world. For atomic and spatial tasks, the approach accelerates inference with a performance degradation of only 0.0%~3.4% compared to the unquantized model. In composite sequential tasks, the sensitivity-aware switching preserves manipulation accuracy during physical interactions, completing tasks with a 66.7% success rate.

### C. Ablation Study

We perform an ablation study on the LIBERO-Spatial suite to evaluate the contribution of each component in *DyQ-VLA* (Tab. III). Relying solely on the static 4-bit (W4A4) quantization degrades the success rate by 15.5% due to accumulated errors in fine-grained manipulation phases. Introducing the kinematic-guided bit allocation strategy restores the success rate to 85.0% by dynamically requesting higher bit-widths during high sensitivity steps. However, this dynamic switching mechanism introduces a latency overhead of 16.8 ms due to high-precision arithmetic and context switching. To mitigate this, the mixed-precision backend assigns W4A2

TABLE I  
SIMULATION RESULTS OF *DyQ-VLA*

Env.	Method	Type	Prec.	SR (%)	Spd.	Mem. (GB)
Goal	FP Model	Stat.	BF16	79.2	1.00×	15.2
	SmoothQuant	Stat.	W4A4	69.6	<b>1.54</b> ×	4.7
	QVLA	Stat.	W4A4	<b>78.8</b>	1.49×	<b>4.3</b>
	<i>DyQ-VLA</i> (Ours)	Dyn.	<b>W4AX</b>	78.5	1.48×	4.7
Object	FP Model	Stat.	BF16	88.4	1.00×	15.2
	SmoothQuant	Stat.	W4A4	73.2	<b>1.49</b> ×	4.7
	QVLA	Stat.	W4A4	87.6	1.44×	<b>4.3</b>
	<i>DyQ-VLA</i> (Ours)	Dyn.	<b>W4AX</b>	<b>87.8</b>	1.47×	4.7
Spatial	FP Model	Stat.	BF16	84.7	1.00×	15.2
	SmoothQuant	Stat.	W4A4	69.2	<b>1.59</b> ×	4.7
	QVLA	Stat.	W4A4	84.4	1.53×	<b>4.3</b>
	<i>DyQ-VLA</i> (Ours)	Dyn.	<b>W4AX</b>	<b>84.7</b>	1.51×	4.7
Long	FP Model	Stat.	BF16	53.7	1.00×	15.2
	SmoothQuant	Stat.	W4A4	40.9	1.47×	4.7
	QVLA	Stat.	W4A4	53.0	1.42×	<b>4.3</b>
	<i>DyQ-VLA</i> (Ours)	Dyn.	<b>W4AX</b>	<b>53.4</b>	<b>1.49</b> ×	4.7

TABLE II  
REAL-WORLD RESULTS OF *DyQ-VLA*

Task Category	FP Model (SR)	<i>DyQ-VLA</i> (SR)	Speedup
Atomic Grasping	<b>86.7%</b>	86.7%	<b>1.43</b> ×
Spatial Displacement	<b>76.7%</b>	73.3%	1.32×
Composite Sequential	<b>70.0%</b>	66.7%	1.38×

TABLE III  
ABLATION STUDIES OF *DyQ-VLA* ON LIBERO-SPATIAL BENCHMARK

Components	SR (%)	Lat. (ms)	Mem. (GB)
Static W4A4	69.2	<b>84.9</b>	4.7
+ Kinematic Dispatch	<b>85.0</b> ↑15.8	101.7 ↑16.8	4.8 ↑0.1
+ Mixed-Precision	84.8 ↓0.2	93.5 ↓8.2	<b>4.7</b> ↓0.1
+ Async Engine (Full)	84.7 ↓0.1	89.4 ↓4.1	4.7 -

states during stable phases to reclaim 8.2 ms of latency caused by memory bandwidth bottlenecks. Furthermore, by decoupling the dispatcher via the asynchronous computation flow, *DyQ-VLA* hides an additional 4.1 ms of scheduling overhead. This integration pushes the overall system speedup to  $1.51\times$  and achieves a favorable Pareto frontier between inference latency and task success rate.

### D. Discussion

1) *Hyper-Parameters Analysis*: System efficiency and accuracy depend on the sliding window sizes ( $W_{\text{macro}}$  and  $W_{\text{micro}}$ ) and the accuracy threshold  $\theta_{\text{fp}}$ . To smooth high-frequency noise while capturing kinematic trends, we employ a dual-window approach with  $W_{\text{macro}} = 10$  and  $W_{\text{micro}} = 5$ . This distinction allows the system to harmonize stable macroscopic trends with transient microscopic spikes.

As shown in Fig. 7, we evaluate the impact of varying  $\theta_{\text{fp}}$  on the success rate and speedup. A higher threshold relaxes the accuracy constraint, allocating lower bit-widths more frequently. While this maximizes the acceleration ratio up to  $1.59\times$ , it compromises manipulation accuracy and leads to a 15.4% decline in the success rate during complex tasks. Conversely, an overly low threshold triggers the full-precision fallback too frequently, diminishing the latency gains of quantization. Based on this trade-off, we identify  $\theta_{\text{fp}} = 0.5$  as the optimal inflection point for balanced performance.

TABLE IV  
OVERHEAD OF THE PROPOSED  $DyQ$ -VLA FRAMEWORK.

System Component	Temporal Cost	Spatial Cost
Kinematic Metric Eval.	< 0.5 ms	~1.2 KB
Dynamic Dispatcher	<b>0 ms</b> (Async)	~0.1 KB
History Buffer Maint.	–	< 64 KB
<b>Total System Impact</b>	<b>Hidden</b>	<b>&lt; 0.1 MB</b>

2) **Overhead Breakdown:** A design principle of  $DyQ$ -VLA is minimizing the operational overhead inherent in dynamic neural networks. Tab. IV breaks down the system overhead into temporal and spatial dimensions. Dynamic switching traditionally incurs delays due to real-time metric computation and operator scheduling bottlenecks, such as frequent kernel launches. Unlike methods requiring expensive online feature evaluation, our lightweight scalar arithmetic on the CPU takes less than 0.5 ms. By executing this concurrently with the visual prefill phase on the GPU, the asynchronous pipeline hides the temporal scheduling cost. For spatial overhead, maintaining stateful history buffers for kinematics operates on one-dimensional data arrays. This implementation occupies less than 64 KB of memory, preserving the 10.5 GB memory reduction achieved by the static-weight paradigm compared to the BF16 baseline.

## VII. CONCLUSION

In this paper, we propose  $DyQ$ -VLA, a dynamic quantization framework for real-time Vision-Language-Action (VLA) edge deployment. By leveraging a sensitivity-aware switching strategy based on kinematic metrics,  $DyQ$ -VLA effectively monitors temporal-dynamic quantization sensitivity. Furthermore, we propose a kinematic-guided bit allocation module to assign optimal bit-widths for manipulation accuracy. Experiments validate  $DyQ$ -VLA's efficient performance, achieving speedups of  $1.49\times$  in simulation and up to  $1.43\times$  in the real world. Notably, it requires only 30.9% of the memory footprint while maintaining 99.5% performance, establishing a novel paradigm for real-time edge deployment.

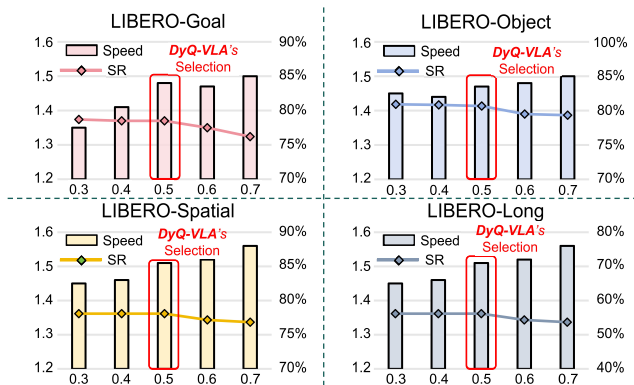


Fig. 7. Discussion of Hyper-Parameter  $\theta_{fp}$  in  $DyQ$ -VLA

## REFERENCES

- [1] R. Sapkota, Y. Cao, K. I. Roumeliotis, and M. Karkee, "Vision-language-action models: Concepts, progress, applications and challenges," *arXiv preprint arXiv:2505.04769*, 2025.
- [2] Z. Yu, B. Wang, P. Zeng, H. Zhang, J. Zhang, L. Gao, J. Song, N. Sebe, and H. T. Shen, "A survey on efficient vision-language-action models," *arXiv preprint arXiv:2510.24795*, 2025.
- [3] M. J. Kim, K. Pertsch, S. Karamcheti, T. Xiao, A. Balakrishna, S. Nair, R. Rafailov, E. Foster, G. Lam, P. Sanketi, *et al.*, "Openvla: An open-source vision-language-action model," *arXiv preprint arXiv:2406.09246*, 2024.
- [4] B. Zitkovich, T. Yu, S. Xu, P. Xu, T. Xiao, F. Xia, J. Wu, P. Wohlhart, S. Welker, A. Wahid, *et al.*, "Rt-2: Vision-language-action models transfer web knowledge to robotic control," in *Conference on Robot Learning*. PMLR, 2023, pp. 2165–2183.
- [5] Physical Intelligence, K. Black, N. Brown, J. Darphinian, K. Dhabalia, D. Driess, A. Esmail, M. Equi, C. Finn, N. Fusai, *et al.*, " $\pi_0.5$ : a vision-language-action model with open-world generalization," *arXiv preprint arXiv:2504.16054*, 2025.
- [6] X. Pei, Y. Chen, S. Xu, Y. Wang, Y. Shi, and C. Xu, "Action-aware dynamic pruning for efficient vision-language-action manipulation," in *The Fourteenth International Conference on Learning Representations*, 2026. [Online]. Available: <https://openreview.net/forum?id=ea6j8k8Rnw>
- [7] Y. Li, Y. Meng, Z. Sun, K. Ji, C. Tang, J. Fan, X. Ma, S.-T. Xia, Z. Wang, and W. Zhu, "SP-VLA: A joint model scheduling and token pruning approach for VLA model acceleration," in *The Fourteenth International Conference on Learning Representations*, 2026. [Online]. Available: <https://openreview.net/forum?id=RwdGhJpIC>
- [8] J. Cao, Q. Zhang, P. Jia, X. Zhao, B. Lan, X. Zhang, Z. Li, X. Wei, S. Chen, L. Li, *et al.*, "Fastdrivevla: Efficient end-to-end driving via plug-and-play reconstruction-based token pruning," *arXiv preprint arXiv:2507.23318*, 2025.
- [9] S. Wang, R. Yu, Z. Yuan, C. Yu, F. Gao, Y. Wang, and D. F. Wong, "Spec-vla: speculative decoding for vision-language-action models with relaxed acceptance," in *Proceedings of the 2025 Conference on Empirical Methods in Natural Language Processing*, 2025, pp. 26 916–26 928.
- [10] S. Xu, Y. Wang, C. Xia, D. Zhu, T. Huang, and C. Xu, "VLA-cache: Efficient vision-language-action manipulation via adaptive token caching," in *The Thirty-ninth Annual Conference on Neural Information Processing Systems*, 2025. [Online]. Available: <https://openreview.net/forum?id=QZYZ0Xm58q>
- [11] Y. Yang, Y. Wang, Z. Wen, L. Zhongwei, C. Zou, Z. Zhang, C. Wen, and L. Zhang, "Efficientvla: Training-free acceleration and compression for vision-language-action models," *arXiv preprint arXiv:2506.10100*, 2025.
- [12] Y. Yue, Y. Wang, B. Kang, Y. Han, S. Wang, S. Song, J. Feng, and G. Huang, "Deer-vla: Dynamic inference of multimodal large language models for efficient robot execution," *Advances in Neural Information Processing Systems*, vol. 37, pp. 56 619–56 643, 2024.
- [13] R. Zhang, M. Dong, Y. Zhang, L. Heng, X. Chi, G. Dai, L. Du, Y. Du, and S. Zhang, "Mole-vla: Dynamic layer-skipping vision language action model via mixture-of-layers for efficient robot manipulation," *arXiv preprint arXiv:2503.20384*, 2025.
- [14] W. Song, J. Chen, P. Ding, Y. Huang, H. Zhao, D. Wang, and H. Li, "Ceed-vla: Consistency vision-language-action model with early-exit decoding," *arXiv preprint arXiv:2506.13725*, 2025.
- [15] M. Shukor, D. Aubakirova, F. Capuano, P. Kooijmans, S. Palma, A. Zouitine, M. Aractingi, C. Pascal, M. Russi, A. Marafioti, *et al.*, "Smolvla: A vision-language-action model for affordable and efficient robotics," *arXiv preprint arXiv:2506.01844*, 2025.
- [16] J. Wen, Y. Zhu, J. Li, M. Zhu, Z. Tang, K. Wu, Z. Xu, N. Liu, R. Cheng, C. Shen, *et al.*, "Tinyvla: Towards fast, data-efficient vision-language-action models for robotic manipulation," *IEEE Robotics and Automation Letters*, 2025.
- [17] J. Liu, M. Liu, Z. Wang, P. An, X. Li, K. Zhou, S. Yang, R. Zhang, Y. Guo, and S. Zhang, "Robomamba: Efficient vision-language-action model for robotic reasoning and manipulation," *Advances in Neural Information Processing Systems*, vol. 37, pp. 40 085–40 110, 2024.
- [18] E. Frantar, S. Ashkboos, T. Hoefler, and D. Alistarh, "GPTQ: Accurate post-training compression for generative pretrained transformers," *arXiv preprint arXiv:2210.17323*, 2022.

- [19] J. Lin, J. Tang, H. Tang, S. Yang, W.-M. Chen, W.-C. Wang, G. Xiao, X. Dang, C. Gan, and S. Han, "Awq: Activation-aware weight quantization for llm compression and acceleration," in *MLSys*, 2024.
- [20] Z. Guan, H. Huang, Y. Su, H. Huang, N. Wong, and H. Yu, "Aptq: Attention-aware post-training mixed-precision quantization for large language models," in *Proceedings of the 61st ACM/IEEE Design Automation Conference*, 2024, pp. 1–6.
- [21] G. Xiao, J. Lin, M. Seznec, H. Wu, J. Demouth, and S. Han, "SmoothQuant: Accurate and efficient post-training quantization for large language models," in *Proceedings of the 40th International Conference on Machine Learning*, 2023.
- [22] Y. Xu, Y. Yang, Z. Fan, Y. Liu, Y. Li, B. Li, and Z. Zhang, "Qvla: Not all channels are equal in vision-language-action model's quantization," 2026. [Online]. Available: <https://arxiv.org/abs/2602.03782>
- [23] H. Fang, Y. Liu, Y. Du, L. Du, and H. Yang, "Sqap-vla: A synergistic quantization-aware pruning framework for high-performance vision-language-action models," *arXiv preprint arXiv:2509.09090*, 2025.
- [24] B. Liu, Y. Zhu, C. Gao, Y. Feng, Q. Liu, Y. Zhu, and P. Stone, "Libero: Benchmarking knowledge transfer for lifelong robot learning," *arXiv preprint arXiv:2306.03310*, 2023.
- [25] Z. Zheng, Z. Mao, M. Li, J. Chen, X. Sun, Z. Zhang, D. Cao, H. Mei, and X. Chen, "Kerv: Kinematic-rectified speculative decoding for embodied vla models," 2026. [Online]. Available: <https://arxiv.org/abs/2603.01581>